plot of the one-electron oxidation potentials versus N^{-1} exhibits good linearity. The intercept (−0.38 V) of the plot may be assigned for the one-electron oxidation potential of the "infinite" fused porphyrin polymer.

In spite of their remarkable properties, including extremely low HOMO-LUMO (highest occupied/lowest unoccupied molecular orbital) gaps, low one-electron oxidation potentials, and rigid and giant molecular size, the triply linked arrays are stable in air and easily manipulated, and should prove useful for studies on the vibronic coupling of organic molecules. They may also find use as conducting molecular wires and in molecular-scale electronic devices. In addition, the unusual photophysical and electrochemical properties of these fused porphyrin arrays suggest potential avenues for further investigation, including the development of near-IR and IR sensors and dyes, and materials for nonlinear optics and spin ordering.

References and Notes

1. R. E. Martin, F. Diederich, *Angew. Chem. Int. Ed.* **38**, 1351 (1999).
2. J. Chen, M. A. Reed, A. M. Rawlett, J. M. Tour, *Science* **286**, 1550 (1999).
3. G. Stegeman, P. Likamwa, *Nonlinear Optical Materials and Devices for Applications in Information Technology*, A. Miller, K. R. Welford, B. Daino, Eds. (Kluwer, Dordrecht, Netherlands, 1995), vol. 289, pp. 285–320.
4. E. Clar, *Ber. Dtsch. Chem. Ges.* **69**, 607 (1936).
5. H. Kuhn, *J. Chem. Phys.* **17**, 1198 (1949).
6. L. M. Tolbert, X. Zhao, *J. Am. Chem. Soc.* **119**, 3253 (1997).
7. D. P. Arnold, G. A. Hearth, *J. Am. Chem. Soc.* **115**, 12197 (1993).
8. V. S.-Y. Lin, S. G. DiMagno, M. J. Therien, *Science* **264**, 1105 (1994).
9. H. L. Anderson, *Chem. Commun.* 2323 (1999).
10. M. J. Crossley, P. L. Burn, *J. Chem. Soc. Chem. Commun.* 1569 (1991).
11. M. G. H. Vicente, L. Jaquinod, K. M. Smith, *Chem. Commun.* 1771 (1999).
12. A. Tsuda, A. Nakano, H. Furuta, H. Yamochi, A. Osuka, *Angew. Chem. Int. Ed.* **39**, 558 (2000).
13. A. Tsuda, H. Furuta, A. Osuka, *Angew. Chem. Int. Ed.* **39**, 2549 (2000).
14. N. Aratani, A. Osuka, Y. H. Kim, D. H. Jeong, D. Kim, *Angew. Chem. Int. Ed.* **39**, 1458 (2000).
15. Recently, we obtained the x-ray crystal structures for *meso-meso*–linked diporphyrin and triporphyrin, both of which display the almost perpendicular conformation of the neighboring porphyrins.
16. The shorter arrays **13**, **14**, and **15** were fully characterized by their ^{1}H nuclear magnetic resonance (NMR) and matrix-assisted laser-desorption/ionization time-of-flight (MALDI-TOF) mass spectroscopy (MS). It proved difficult to obtain satisfactorily resolved ^{1}H NMR spectra for longer arrays owing to their poor solubility, but their MALDI-TOF MS spectra indicated clustering peaks corresponding to dimers of ionized arrays. In the gel-permeation chromatography, all the triply linked porphyrin arrays exhibit a single band with a retention time that is progressively slower than those of the starting *meso-meso*–linked porphyrin arrays, indicating their discreteness and homogeneity. In addition, preliminary scanning tunneling microscopy measurements on these arrays revealed a roughly rectangular shape for hexamer **17** (2 nm by 5 nm) and octamer **18** (2 nm by 6.5 nm), consistent with the expected molecular shapes (*18*).
17. Although the assignment of these absorption bands (I, II, and III) has not yet been fixed, it may be possible to qualitatively understand these spectral characteristics on the basis of the well-established Gouterman four-orbital theoretical model for the absorption spectra of porphyrins (*19*, *20*). In this theory, the B and Q bands both arise from π-π^* transitions and can be explained in terms of a linear combination of transitions from a_{1u} and a_{2u} HOMO orbitals to a degenerate pair of e_{gx} and e_{gy} LUMO orbitals. The two HOMO orbitals have the same energy, and the configurational interaction results in two bands with very different intensities and wavelengths: the intense, short-wavelength B band and the weak, long-wavelength Q band. However, the fused connection causes a significant perturbation that breaks down the degeneracy of the e_{gx} and e_{gy} orbitals. It may thus be pertinent to assign the bands I and II to allowed transitions along the shorter and longer molecular axes of the rectangular fused porphyrin arrays, respectively. Band III may thus correspond to a formally forbidden transition such as Q-bands in the D_4-symmetry Zn(II) porphyrin monomer, because these absorption bands become increasingly intensified upon the increase of the arrays.
18. A. Takagi, Y. Yanagawa, T. Matsumoto, T. Kawai, A. Tsuda, A. Osuka, unpublished results.
19. M. Gouterman, *J. Mol. Spectrosc.* **6**, 138 (1961).
20. O. Bilsel *et al.*, *J. Am. Chem. Soc.* **114**, 6528 (1992).

21. Supported by Grants-in-Aid for Scientific Research from the Ministry of Education, Science, Sports and Culture of Japan (11223205, 12440196, and 12874076) and by CREST (Core Research for Evolutional Science and Technology) of Japan Science and Technology Corporation. A.T. was supported by a Japan Society for the Promotion of Science Research Fellowship for Young Scientists.

5 February 2001; accepted 22 May 2001

Approach to High-Resolution ex Situ NMR Spectroscopy

Carlos A. Meriles, Dimitris Sakellariou, Henrike Heise, Adam J. Moulé, Alexander Pines*

Nuclear magnetic resonance (NMR) experiments are typically performed with samples immersed in a magnet shimmed to high homogeneity. However, there are many circumstances in which it is impractical or undesirable to insert objects or subjects into the bore of a high-field magnet. Here we present a methodology based on an adaptation of nutation echoes that provides resolved spectra in the presence of matched inhomogeneous static and radiofrequency fields, thereby opening the way to high-resolution ex situ NMR. The observation of chemical shifts is regained through the use of multiple-pulse sequences of correlated, composite *z*-rotation pulses, producing resolved NMR spectra of liquid samples.

The practice of high-resolution NMR spectroscopy usually involves the use of large magnets producing homogeneous static (B_0) fields. Experiments performed inside such magnets yield information about molecular structure and dynamics through the observation of interactions such as chemical shifts and scalar couplings. These features make in situ NMR a powerful analytical tool used to study such diverse questions as the metabolism of plants and organisms (*1*), the dynamics of geological processes (*2*), and the characterization of technologically important new materials (*3*). For many applications, it would be useful if a mobile magnet could be scanned over an otherwise inaccessible object or subject in order to acquire magnetic resonance information. The advantage of such ex situ analysis is that limitations of sample size

Materials Sciences Division, Lawrence Berkeley National Laboratory and Department of Chemistry, University of California, Berkeley, CA 94720, USA.

*To whom correspondence should be addressed.

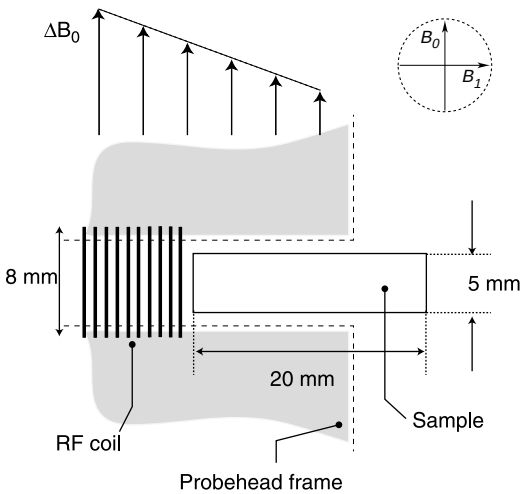

Fig 1. Schematic representation of the experimental setup. A single solenoid serves to irradiate and detect the NMR proton signal from a sample of trans-2-pentenal contained in a glass tube inside the bore of a superconducting magnet. To simulate the environment of an ex situ surface coil, we placed the sample completely outside the solenoid central cavity. An imaging coil set (not displayed in the figure) is used to generate a linear gradient of the static field along the solenoid axis. All experiments were carried out in a super-widebore imaging magnet with an Infinity Varian spectrometer operating at 179.12-MHz proton frequency and a home-built imaging probehead with three perpendicular gradient coils.

and transportability no longer prevail, but an accompanying handicap is that the magnetic fields are necessarily spatially inhomogeneous. As a consequence, the NMR spectra become broadened to the extent that resolution and associated chemical shift information are hidden, even if echo sequences are used that enhance detection sensitivity by periodically refocusing the signal (*4*). Schemes designed to extract spin-lattice and transverse relaxation times as diagnostic indicators of composition in the absence of spectral resolution have been developed with broad applications from material science and food technology to biomedicine (*5*). In a different context, several schemes involving coherence transfer (*6*), cross relaxation (*7*) correlation spectroscopy (*8*), and intermolecular dipolar fields (*9*) have been used in some circumstances to mitigate the effects of inhomogeneous fields. It has also been shown that nutation echoes can be generated by matching radiofrequency (rf) gradients with static field gradients over a region of the sample (*10*, *11*), allowing the measurement of diffusion and volume-selective imaging (*12*).

We now present preliminary results that show that spectral resolution can actually be recovered and full chemical shift information can be obtained for a sample subjected to strong static field inhomogeneity and excited by a surface coil. The methodology described below involves the use of trains of composite *z*-rotation pulses inducing nutation echoes over a region of matched rf and static field gradients.

A brief survey of our experimental setup is shown in Fig. 1. To emulate ex situ conditions inside the magnet bore, we produced a static B_0 field gradient by driving current into the *x*-gradient coils of the probehead. The sample was then attached outside the rf coil. Figure 2 displays ^{1}H (proton) NMR spectra of trans-2-pentenal in a tube of 5-mm diameter and 2-cm length. The "normal" one-pulse free induction decay (FID) proton NMR spectrum in a rather homogeneous B_0 field (Fig. 2A) exhibits five resolved lines at 9.5, 7.0, 6.1, 2.4, and 1.1 parts per million (ppm) with relative intensities of 1:1:1:2:3 that correspond, respectively, to the formylic, the two olefinic, and the two aliphatic protons. In the presence of a B_0 gradient of 0.12 mT/cm, the inhomogeneously broadened spectrum (Fig. 2B) is rendered featureless and extends over a range of 20 ppm—twice the normal chemical shift range of proton NMR spectra. In contrast, the spectrum obtained by the use of an appropriately designed train of composite *z*-rotation pulses (Fig. 2C) in the presence of the same field inhomogeneity revives the spectroscopic resolution of all five proton NMR lines.

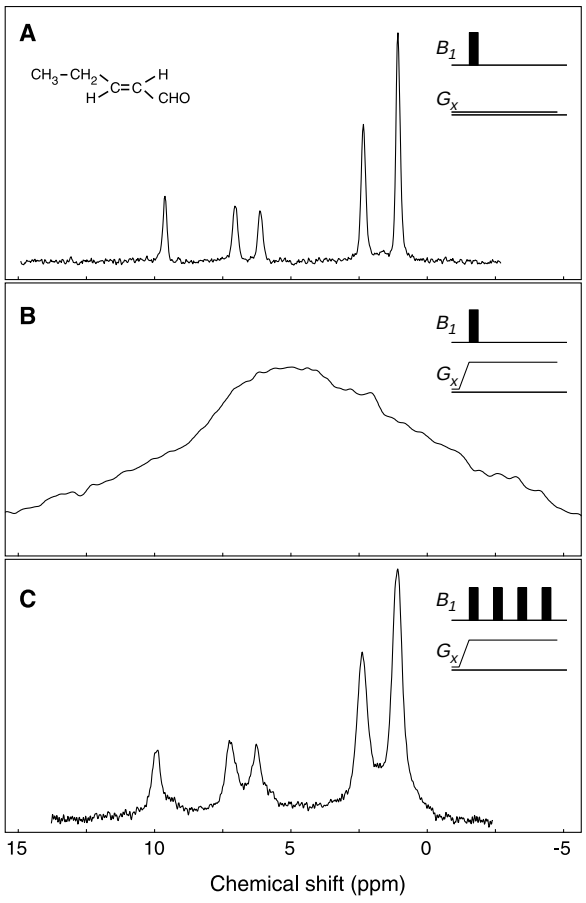

Fig. 2. (**A**) One-pulse proton spectrum of trans-2-pentenal (eight scans). The linewidth (~40 Hz) is dominated by the intrinsic residual inhomogeneity of the magnetic field. (**B**) Spectrum of trans-2-pentenal (64 scans, 2.2 kHz full width at half maximum line broadening) in the presence of a linear static field gradient of 0.12 mT/cm (~5 kHz/cm) along the sample axis. An exponential apodization of 50 Hz was applied to enhance the signal to noise ratio. (**C**) Proton spectrum obtained with the refocusing sequence of Fig. 3B after 64 scans, in the presence of the same field gradient. Constant-rotation composite $\pi/2$ pulses were implemented by the series $(2\gamma)_{97.2}(4\gamma)_{291.5}(2\gamma)_{97.2}(\gamma)_0$, where γ represents a nominal $\pi/2$ pulse (*13*). The total duration was 117 μs; τ_β, the length of the β pulse, was 23 μs for an evolution time τ_{dw} set at 250 μs. After processing the FID, the frequency units were shifted so that the position of the most intense peak matched the corresponding peak observed in (A). Even though the linewidth is slightly increased, all nonequivalent proton resonances are resolved and the full chemical shift information is recovered.

The basic mechanism underlying the use of composite *z*-rotation pulses can be visualized by means of a classical vector diagram in the rotating frame (Fig. 3A). For spins with the same chemical shift, different Larmor frequencies $\omega_0(\vec{r})$ throughout the sample give rise to progressive dephasing during a free evolution period. At any stage, this loss of coherence can be reversed if a proper position-dependent phase correction is applied. However, by doing so, phase differences accumulated during the evolution and arising from the chemical shifts and scalar *J* couplings are maintained. Such a position-dependent phase correction can be accomplished by the use of a *z*-rotation pulse $[\beta(\vec{r})]_{-z} = (\pi/2)_y[\beta(\vec{r})]_x(\pi/2)_{-y}$. Even in the presence of rf inhomogeneity and offset, carefully designed constant-rotation composite ($\pi/2$) pulses (*13*) ensure a 90° rotation for a major part of the sample contributing to the induced signal. However, the rotation angle β depends on the local rf strength $\omega_1(\vec{r})$ and for a fixed pulse length τ_β, the phase correction at each site is given by $\beta(\vec{r}) = \omega_1(\vec{r})\tau_\beta$. If *k* denotes the (position-independent) ratio between the static field and the rf gradients, the length of the β pulse for a given free evolution interval τ_{dw} is selected so that $\tau_\beta = k\tau_{dw}$. By this means, a nutation echo takes place at a time $\tau_{dw}/2$ after the *z* pulse is applied (see Fig. 3A). Accounting for an overall but constant phase shift $\omega_{10}\tau_\beta$, the measured signal at this single point is insensitive to field inhomogeneities but fully preserves the chemical shift evolution during the period τ_{dw}.

A generalization of this principle that combines the repeated application of composite *z*-rotation pulses with stroboscopic acquisition (*14*) enables the direct detection of resolved NMR spectra in inhomogeneous fields (Fig. 3B). In this pulse scheme, the magnetization is initially dephased by a β pulse of duration τ_β before the free evolution period τ_{dw}. At the end of this period, a nutation echo takes place and a single point acquisition is made; immediately after, another constant-rotation composite $\pi/2$ pulse tips the magnetization back onto the *zy* plane and the cycle starts again. The phase shift introduced at each step of the train can be easily corrected by properly changing the phase of the synthesizer or by a frequency shift of the whole spectrum after processing the FID. In either case, this procedure provides a spectrum that, despite strong field inhomogeneities, still contains the full chemical shift information of the sample (*15*).

To a first approximation, the maximum available rf field (in this case, 25 kHz for spins immediately close to the rf coil) sets a practical limit on the gradient strength that can be handled: The higher the field inhomogeneity, the greater is the rf power required to maintain the β-pulse offset independent in the region of interest. Under the present con-

ditions, resolved spectra in field gradients of up to 0.5 mT/cm (~20 kHz/cm) have been successfully obtained (*16*). Although these values are still small compared with those found in practical applications such as those of the "NMR Mouse" (*5*), much improvement is expected by designing pulse sequences to be less sensitive to offset and by properly matching rf and static field gradients

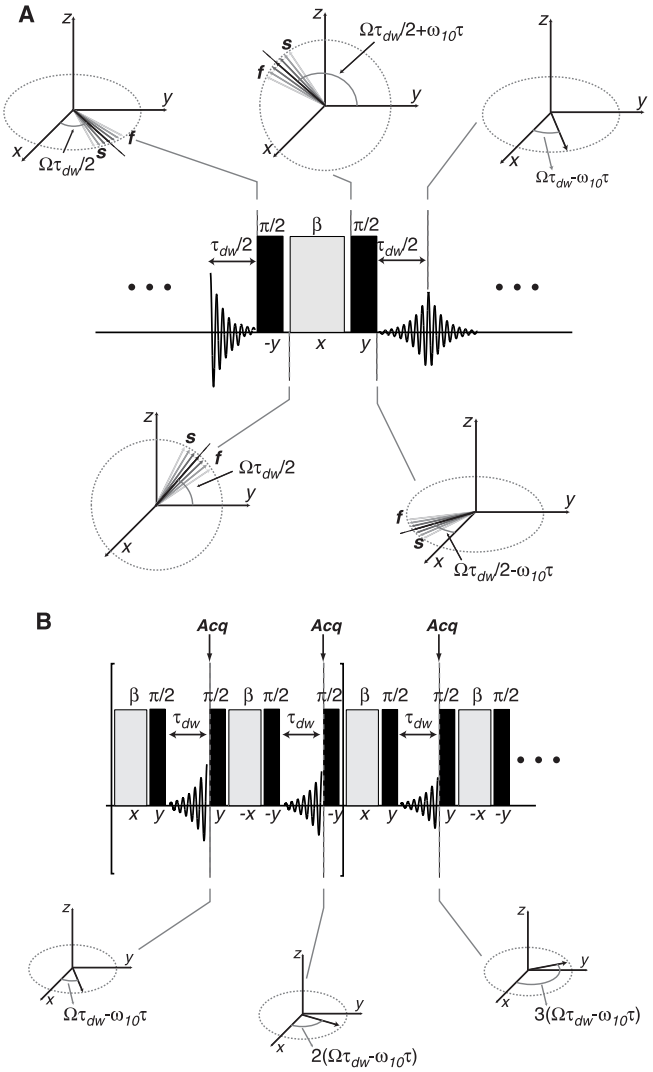

Fig. 3. (**A**) Rotating-frame classical diagram describing spin evolution under a train of *z*-rotation composite pulses. For the sake of clarity, the diagram only depicts nuclear spins with the same chemical shift but spread over different positions along the sample. During a free evolution period, equivalent spins dephase because of the spatial dependence of the Larmor frequency. "Faster" ("slower") spins, located closer to (away from) the excitation coil, have been labeled by a small *f* (s) in the diagram. A position-dependent phase correction is possible through the pulse series $(\pi/2)_{-y}[\beta(\vec{r})]_x(\pi/2)_y$: (Perfect) constant-rotation composite $\pi/2$ pulses tip the spins back and forth between the *xy* and *yz* planes. In the region of the sample where the static and rf field gradients are matched, a $[\beta(\vec{r})]_x$ pulse applied over the proper time period gives rise to an overall phase shift that exactly reverses the relative positions of (chemically equivalent) fast and slow spins and induces a subsequent nutation echo. Because the same phase shift equally affects nuclei with different chemical shifts, the echo amplitude fully preserves the accumulated phase differences between chemically inequivalent spins. (**B**) Pulse train actually used during the experiment. An initial dephasing induced by the pulse $[\beta(\vec{r})]_x$ is refocused during the free evolution (or dwell time) period. A one-point acquisition takes place at the nutation echo maximum, just before the next $(\pi/2)$ pulse. At each step in the train, a phase alternation is performed to compensate for undesired evolution during the rf irradiation. The entire rf sequence—indicated by surrounding brackets in the drawing—is repeated, with stroboscopic detection providing the inhomogeneity-free free induction decay. The constant phase shift $\omega_{10}\tau_\beta$ remaining at each step of the train can be corrected by sequentially adjusting the phase of the rf pulses or by a shift of the reference frequency in the measured spectrum after data processing.

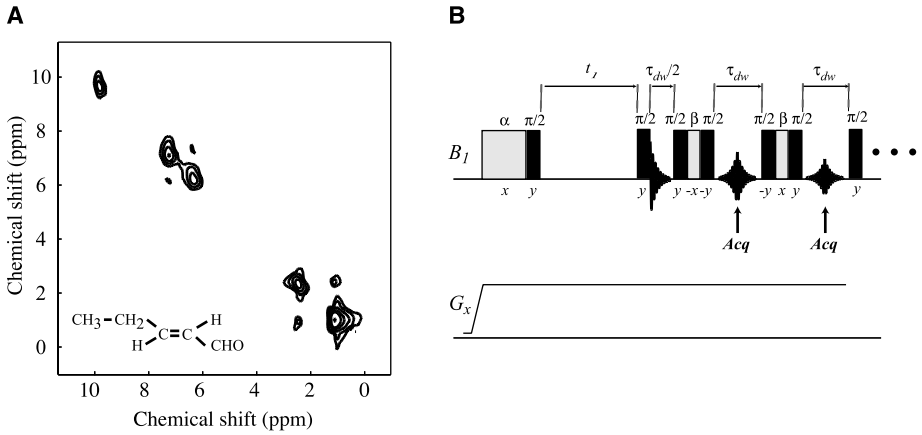

Fig. 4. (**A**) Two-dimensional correlation spectrum (absolute value mode) of trans-2-pentenal obtained through (**B**) an adapted COSY sequence under conditions identical to those of Fig. 2B. A linear static field gradient of 0.12 mT/cm (~5 kHz/cm) along the sample axis spreads the Larmor frequencies in both dimensions over a range of 20 ppm, and no relevant spectroscopic information can be recorded with a standard experiment. In the present case, however, the evolution period is made insensitive to field inhomogeneities by the use of a pulse $[\alpha(\vec{r})]_x$ before the standard $(\pi/2)_y$ excitation pulse. The duration of $[\alpha(\vec{r})]_x$ is sequentially incremented in a manner proportional to t_1. The ratio is adjusted so that the next $(\pi/2)_y$ mixing pulse occurs synchronously with the nutation echo. In the direct dimension, the detection is made stroboscopically in a way similar to that of Fig. 2C. After a time $\tau_{dw}/2$, a composite *z* pulse is applied and the dephasing due to inhomogeneities is reversed. A single point acquisition takes place at the expected nutation echo time in between the pulses of the train. All diagonal peaks as well as most of the cross peaks for *J*-coupled protons are regained (a higher level contour for peaks belonging to aliphatic protons has been used to improve resolution). The number of increments for t_1 was 64 in steps of 250 μs. This was also the value assigned to τ_{dw} ensuring the same bandwidth for both dimensions. The number of scans for each evolution time t_1 was 8.

over more extended regions. In this regard, composite β pulses with a properly designed functional dependence of rotation amplitude on ω_1 should lead to improved refocosing for general of profiles.

The extension of these principles to multidimensional spectroscopy is straightforward, and Fig. 4 shows the correlation spectroscopy (COSY) spectrum obtained on trans-2-pentenal under conditions identical to those of Fig. 2 with the field gradients applied. Cross peaks indicating *J*-coupled proton spins are still recognizable even though the field inhomogeneity is sufficient to completely erase any spectroscopic information. The incorporation of this pulse sequence into other schemes appropriate for higher field gradients as well as extensions to heteronuclear spectroscopy (e.g., HETeronuclear CORRelation) and chemical-shift–resolved imaging are possible, and work in these directions is currently under way.

We not that the full spectroscopic information of a sample can still be obtained if a period of free evolution under a static field gradient is followed by another period with the field gradient reversed. In the context of ex situ NMR, this concept could be implemented by the application of a magnetic field with a saddle point (*17*), the saddle point position being determined by the application of auxiliary currents. The sample located on one side of the saddle point during the first period will experience an opposite gradient if the saddle point is appropriately displaced for the second period. This procedure represents an extension of the sequence discussed above, now based on the degree of correlation attainable with static field matching on both sides of the saddle point. Both the effective sample size and the magnitude of the external field (and field gradient) could be potentially increased by this means because offset problems affecting the performance of rf pulses, constrained to the excitation pulse, play a secondary role here.

Finally, we mention a possible extension of the field variation concept that involves the use of several coils to generate a magnetic field spinning at the magic angle (*18*, *19*) with respect to static ex situ samples. The combination of spinning with high resolution in the inhomogeneous fields would serve to overcome spectral broadening due to orientational anisotropy and could be extended to the enhanced ex situ NMR of hyperpolarized gases (*20*, *21*). Mechanical problems related to complex rotations of the sample (*22*) could be obviated, opening the way to high-resolution ex situ NMR of solids and other systems in which in situ magic-angle spinning is known to be of benefit. Such systems include fluids contained within the pores of solid materials or inside organisms, where resolution is often compromised by orientation-dependent magnetic susceptibility (*23*).

References and Notes

1. J. J. H. Ackerman, T. H. Grove, G. G. Wong, D. G. Gadian, G. K. Radda, *Nature* **283**, 167 (1980).
2. J. F. Stebbins, I. Farnan, *Science* **245**, 257 (1989).
3. S. Frank, P. C. Lauterbur, *Nature* **363**, 334 (1993).
4. M. D. Hürlimann, D. D. Griffin, *J. Magn. Reson.* **143**, 120 (2000).
5. B. Blümich *et al.*, *Magn. Reson. Imag.* **16**, 479 (1998).
6. D. P. Weitekamp, J. R. Garbow, J. B. Murdoch, A. Pines, *J. Am. Chem. Soc.* **103**, 3578 (1981).
7. J. J. Balbach *et al.*, *Chem. Phys. Lett.* **277**, 367 (1997).
8. L. D. Hall, T. J. Norwood, *J. Am. Chem. Soc.* **109**, 7579 (1987).
9. W. Richter, S. Lee, W. S. Warren, Q. He, *Science* **267**, 654 (1995).
10. A. Jershow, *Chem. Phys. Lett.* **296**, 466 (1998).
11. A. Sharfenecker, I. Ardelean, R. Kimmich, *J. Magn. Reson.* **148**, 363 (2001).
12. I. Ardelean, R. Kimmich, A. Klemm, *J. Magn. Reson.* **146**, 43 (2000).
13. M. H. Levitt, *The Encyclopedia of NMR* (Wiley, London, 1997), pp. 1396–1411.
14. Point-by-point acquisition with a sequential increment of the β-pulse length is conceivable as well. However, as in the Carr-Purcell train, incomplete refocusing due to diffusion is best suppressed by keeping the free evolution time sufficiently short.
15. Closer examination of Fig. 2C shows that the chemical shift scale is slightly enhanced with respect to the conventional spectrum, an effect that arises from the evolution of the nuclear magnetization under the field offset during the composite π/2 pulses. This renders the effective dwell time slightly longer than the free evolution period τ_{dw} used for the Fourier transformation. A correction can be applied by simply rescaling the shift scale. Undesired offset-induced evolution during the rf pulses also leads to spectral artifacts that distort neighboring peaks around the irradiation frequency. However, the results in Fig. 2C show that these effects can be overcome to a great extent by a phase alternation on the composite z-rotation pulses at each step of the pulse train (see Fig. 3B). Further improvement can be obtained by tuning the rf toward lower frequencies (corresponding to spins located farther away from the coil). If the rf field is high enough, this ensures that most nuclei contributing substantially to the signal experience a reduced offset effect during the β pulse.
16. The gradient can be further increased if the composite π/2 pulses are replaced by single pulses of adjustable length. When this length matches the 90° condition for on-resonance nuclei, a highly spatially selective excitation occurs that still provides extremely sharp spectra, with a correspondingly diminished sensitivity.
17. R. L. Kleinberg, A. Sezginer, D. D. Griffin, M. Fukuhara, *J. Magn. Reson.* **97**, 466 (1992).
18. E. R. Andrew, A. Bradbury, R. G. Eades, *Nature* **182**, 1659 (1958).
19. E. R. Andrew, R. G. Eades, *Disc. Faraday Soc.* **34**, 38 (1962).
20. M. S. Albert *et al.*, *Nature* **370**, 199 (1994).
21. G. Navon *et al.*, *Science* **271**, 1848 (1996).
22. B. F. Chmelka, A. Pines, *Science* **246**, 71 (1989).
23. T. M. de Swiet, M. Tomaselli, M. D. Hürlimann, A. Pines, *J. Magn. Reson.* **133**, 385 (1998).

24. We thank J. D. Walls for fruitful discussions and A. H. Trabesinger for kindly reviewing the manuscript. This work was supported by the Director, Office of Science, Office of Basic Energy Sciences, Materials Sciences Division, of the U.S. Department of Energy under contract DE-AC03-76SF00098. C.A.M. acknowledges Consejo Nacional de Investigaciones Científicas y Tecnológicas, Argentina, and H.H. thanks the Humboldt Foundation for support through postdoctoral fellowships.

10 April 2001; accepted 30 May 2001

Regional Climate Impacts of the Northern Hemisphere Annular Mode

David W. J. Thompson[1]* and John M. Wallace[2]

The Northern Hemisphere annular mode (NAM) (also known as the North Atlantic Oscillation) is shown to exert a strong influence on wintertime climate, not only over the Euro-Atlantic half of the hemisphere as documented in previous studies, but over the Pacific half as well. It affects not only the mean conditions, but also the day-to-day variability, modulating the intensity of mid-latitude storms and the frequency of occurrence of high-latitude blocking and cold air outbreaks throughout the hemisphere. The recent trend in the NAM toward its high-index polarity with stronger subpolar westerlies has tended to reduce the severity of winter weather over most middle- and high-latitude Northern Hemisphere continental regions.

The NAM is a planetary-scale pattern of climate variability characterized by an out-of-phase relation or seesaw in the strength of the zonal flow along ~55° and 35°N and accompanied by displacements of atmospheric mass between the Arctic basin and the mid-latitudes centered ~45°N (*1*–*4*). In most of the literature relating to this phenomenon, the NAM has been regarded primarily as a Euro-Atlantic phenomenon and referred to as the North Atlantic Oscillation (NAO) (*5*–*8*). Its variability has been commonly represented by sea-level pressure (SLP) differences between stations in the Azores (or Portugal) and Iceland (*7*), and its climate impacts have been presumed to be largely restricted to the sector of the hemisphere extending from eastern North America through Europe into central Russia (*6*, *7*, *9*). Here, we demonstrate that

[1]Department of Atmospheric Science, Colorado State University, Fort Collins, CO 80523, USA. [2]Department of Atmospheric Sciences, University of Washington, Seattle, WA 98195, USA.

*To whom correspondence should be addressed. E-mail: davet@atmos.colostate.edu